

Two Cycling Centers in One Molecule: Communication by Through-Bond Interactions and Entanglement of the Unpaired Electrons

Maxim V. Ivanov, Sahil Gulania, and Anna I. Krylov*

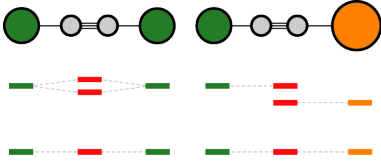
Department of Chemistry, University of Southern California, Los Angeles, California, USA

E-mail: krylov@usc.edu

Abstract

Many applications in quantum information science (QIS) rely on the ability to laser-cool molecules. The scope of applications can be expanded if laser-coolable molecules possess two or more cycling centers, i.e., moieties capable of scattering photons via multiple absorption-emission events. Here we employ equation-of-motion coupled-cluster method for double electron attachment (EOM-DEA-CCSD) to study the electronic structure of hypermetallic molecules with two alkaline earth metals connected by an acetylene linker. The electronic structure of the molecules is similar to that of two separated alkali metals; however, the interaction between the two electrons is weak and largely dominated by through-bond interactions. The communication between the two cycling centers is quantified by the extent of the entanglement of the two unpaired electrons associated with each center. This contribution highlights the rich electronic structure of hypermetallic molecules that may advance various applications in QIS and beyond.

Graphical TOC entry



Many promising applications in quantum information science (QIS),¹⁻⁴ precision measurements,^{5,6} and ultra-cold chemistry⁷⁻⁹ rely on the ability to efficiently laser-cool molecules.^{10,11} Similarly to atoms, molecules are laser-cooled by scattering photons in multiple absorption-emission events. This process of repeated absorption and emission is called optical cycling. In contrast to atoms, the decay of molecular excited states may populate many vibrational and rotational states, owing to multiple degrees of freedom and complex electronic structure. As a result, following a single absorption-emission cycle the system may not return to its starting point to absorb another photon, and the laser cooling becomes inefficient. Thus, molecules suitable for laser cooling should afford electronic transitions giving rise to negligible structural relaxation, i.e., with diagonal Franck-Condon factors (FCFs).¹² Diagonal FCFs can be realized in molecules in which a single unpaired electron is localized at the cycling center (often, an alkaline earth metal, a rare earth metal, or a lanthanide), giving rise to atom-like transitions. Several molecules in this class have been experimentally laser-cooled to (sub-)millikelvin temperatures,¹³⁻²⁰ and many more have been proposed on the basis of electronic structure calculations.²¹⁻²⁹ Particularly noteworthy are breakthroughs by Doyle’s group³⁰ who succeeded to laser-cool SrOH and, more recently, YbOH,⁵ opening possibilities for the cooling of even larger polyatomic molecules with various cycling centers.^{31,32} The ability to laser-cool polyatomic molecules is crucial for progress in this domain: for example, symmetric-top molecules offer new opportunities in the field of quantum computing⁴ and precision measurements.⁶

The scope of possible applications of laser-coolable molecules can be further expanded if multiple cycling centers are incorporated in the same molecule. For example, hypermetallic molecules with two cycling centers, such as YbCCCa and YbCCAl, have been shown to be a versatile platform for state-of-the-art precision measurements.³³ Another interesting class of potentially laser-coolable molecules is hypermetallic neutral and ionic oxides of alkaline earth metals with a general chemical formula AOB, where A and B are the same or different alkaline earth metals. Several possible variants of neutral AOB have been studied spectroscopically and theoretically,³⁴⁻³⁸ and quantum state controlled synthesis of CaOBa⁺ has been recently demonstrated.³⁹ Generalizing the concept of hypermetallic molecules, one can consider a series

of molecular frameworks that would allow engineering laser-coolable molecules with two (or more) cycling centers separated by various linkers (Figure 1).

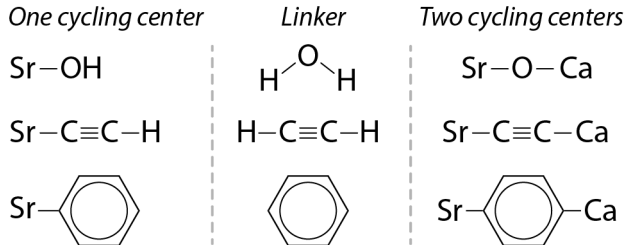


Figure 1: Examples of molecules accommodating one and two cycling centers.

In the context of the rational design of laser-coolable molecules with multiple cycling centers, there is no clear-cut guiding principle for the exact details of electronic structure preferred for a given application. For example, the desired extent of communication between the two centers can vary depending on the task at hand. Thus, it is important to understand how to control the coupling between the centers by structural modifications. The strength of the interaction between the cycling centers can be tuned by using linkers of varied length (Figure 1). One should also keep in mind that the nature of the linker directly impacts the electronic structure of the molecule. In this context, lessons learned from studies of diradicals and polyradicals provide valuable insights.^{40–43} For example, the interplay between the (direct) through-space interaction between the two electrons and the (indirect) through-bond interaction can strongly affect the electronic structure of the molecule. In a representative example, the *para*-benzyne diradical, a considerable through-bond interaction flips the ordering of the frontier orbitals relative to the one expected on the basis of through-space interactions, and the formally antibonding orbital becomes lower in energy than the bonding one.^{44,45}

In this Letter, we investigate the electronic structure of hypermetallic molecules with two cycling centers connected by the acetylene linker: ACCB, where A and B are either the same or different alkaline earth metals (A, B = Mg, Ca, Sr). Main focus is on the strength of the interaction between the two unpaired electrons and how this interaction manifests itself in the underlying electronic structure and experimental observables, such as excitation energies, singlet-triplet energy gaps, excitonic splittings, and oscillator strengths. We also analyze the

underlying wavefunctions in terms of the number of effectively unpaired electrons and the effective number of entangled states.

The main challenge in the first-principle calculations of this class of systems lies in their strong diradical character, which originates from the near-degeneracies of the frontier molecular orbitals and leads to the multiconfigurational wave functions.⁴³ Standard electronic structure methods based on the hierarchical improvements of the single-determinantal Hartree-Fock wave-function fail to accurately describe the electronic structure of diradicals and systems with more unpaired electrons. An elegant and robust solution to this problem is afforded by equation-of-motion coupled-cluster (EOM-CC) methods, which are capable of describing multiconfigurational wave functions in a single-reference framework.^{43,46,47}

Different variants of EOM-CC provide access to different types of target states and different degeneracy patterns. For example, the manifold of low-lying diradical and triradical states can be accessed by the EOM-SF ansatz.⁴⁸⁻⁵⁰ The EOM-SF approach describes the target singlet and triplet ($M_s = 0$) states by spin-flipping excitations from the high-spin triplet ($M_s = 1$) reference state in which the two (near)-degenerate frontier orbitals are singly occupied (Figure 2). The configurations involving single excitations within the singly occupied orbital space form a spin-complete set (the first four configurations in the top panel in Fig. 2), but the single excitations from the singly occupied to virtual space (configurations 5 and 6 in the top panel) lack their spin counterparts, which only appear at the doubly excited level (configurations 7 and 8). The unbalanced treatment of these configurations (5/6 and 7/8) results in spin contamination and deteriorated accuracy. Thus, although EOM-SF treats well the primary diradical manifold (states described by configurations 1-4, such as the lowest singlet and triplet states of the molecules with two cycling centers), it would not be an optimal choice for higher excited states involving excitations outside of the singly occupied space (such as the states responsible for cycling transitions in ACCB).

Alternatively, diradical states of an N -electron system can be accessed by EOM-DEA-CC (EOM-CC for double electron attachment) starting from the closed-shell Ψ_{N-2} reference wavefunction⁵¹ in which both frontier orbitals are unoccupied (Figure 2, bottom). The target

states are produced by the EOM operator, which adds two electrons to Ψ_{N-2} . As one can see, the set of configurations generated by the 2-particle EOM-DEA operator includes both the configurations from the primary diradical manifold and also configurations that involve excitations outside of the singly occupied space. Consequently, EOM-DEA can also describe higher excited diradical states. As long as the closed-shell reference is used, the DEA target states are spin pure. Here we employ EOM-DEA-CC with single and double substitutions (EOM-DEA-CCSD) in which the reference state is described by CCSD and the excitation operators R are of the 2-particle ($2p$) and 3-particle-1-hole ($3p1h$) types:

$$\hat{R}^{+2} = \frac{1}{2} \sum_{ab} r^{ab} b^\dagger a^\dagger + \frac{1}{6} \sum_{iabc} r_i^{abc} c^\dagger b^\dagger a^\dagger i. \quad (1)$$

We used EOM-EA-CCSD (EOM-CCSD with $1p$ and $2p1h$ operators) to compute energies, properties, and structures of the doublet species (ACCH). For the diradical species (ACCB), we used EOM-DEA-CCSD for energies and properties calculations and CCSD/EOM-SF-CCSD (EOM-CCSD with $1h1p$ and $2h2p$ spin-flipping operators) for structures' optimizations.⁵²

The extent of the interaction between the two unpaired electrons can be characterized by concrete physical observables: spectroscopically, by the energy gap between the lowest singlet and triplet state, structurally, by considering the distances between the two centers, or thermochemically, by computing the energy of a hypothetical reaction separating the two centers.^{42,53} Additional insight can be gained from the analysis of the underlying wave-functions,⁴⁵ such as shapes and occupations of natural frontier orbitals and the effective number of unpaired electrons. Although not experimentally measurable, these quantities reflect the bonding patterns imprinted in the electronic structure and related to the structural, spectroscopic, and thermochemical observables. The definition of the effective number of unpaired electrons is grounded in the concept of natural orbitals.⁵⁴ Natural orbitals are the eigenstates of the one-particle reduced density matrix, with the eigenvalues n_i that are non-negative, less than 2, and add up to the total number of electrons; hence, they can be interpreted as orbital occupations. That is, natural orbitals with occupations close to 2 can be described as doubly occupied orbitals,

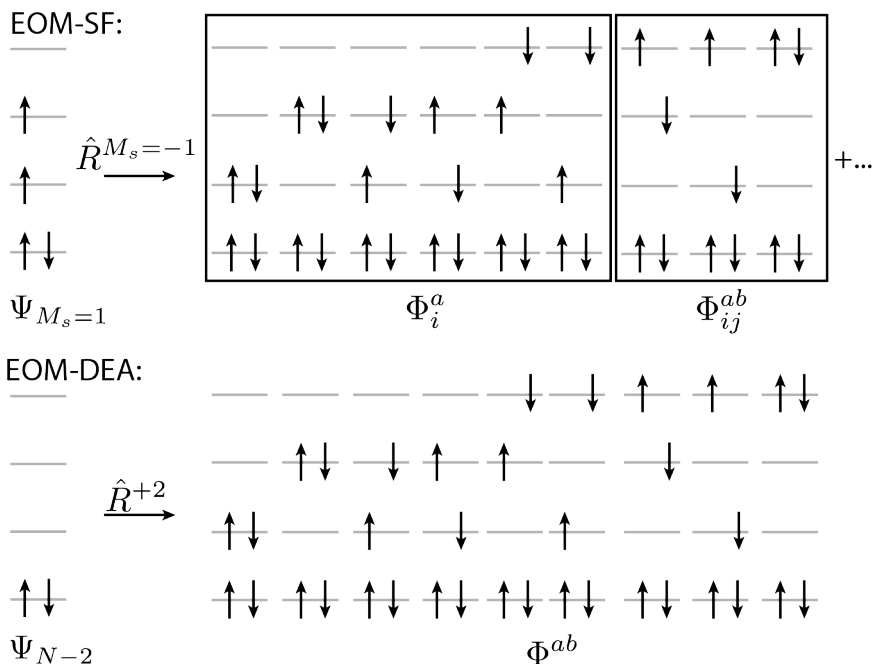


Figure 2: EOM-SF (top) and EOM-DEA (bottom) ansätze allow access to diradical states. In the EOM-SF method, the target low-spin $\Psi_{M_s=0}$ states are reached by applying spin-flipping excitation operator $\hat{R}^{M_s=-1}$ to the high-spin reference $\Psi_{M_s=1}$ state: $\Psi_{M_s=0} = \hat{R}^{M_s=-1}\Psi_{M_s=1}$. Excitations from the doubly occupied orbitals are not shown. In the EOM-DEA method, the target Ψ_N states are reached by applying excitation operator \hat{R}^{+2} , which adds two electrons to the closed-shell reference Ψ_{N-2} with $N - 2$ electrons: $\Psi_N = \hat{R}^{+2}\Psi_{N-2}$. Only configurations generated by the two-particle part of \hat{R}^{+2} are shown.

those with small occupation numbers can be described as unoccupied orbitals, and orbitals with noticeable fractional occupations can be described as natural frontier orbitals. For example, in diradicals, one expects to find two orbitals with occupations close to 1; visualization of these orbitals provides a picture of the states of the unpaired electrons.⁴⁵ There are several ways that can be used to compute an effective number of unpaired electrons from natural occupation numbers and here we rely on the indices introduced by Head-Gordon;⁵⁵ specifically, $n_{u,nl}$

$$n_{u,nl} = \sum_i n_i^2 (2 - n_i)^2, \quad (2)$$

which has been shown to reliably yield values that are consistent with chemical intuition.⁵⁶

To visualize the states of the unpaired electrons we use Dyson orbitals⁵⁷ and natural orbitals.⁵⁴ Electronic transitions are analyzed using natural transition orbitals (NTOs).⁵⁸⁻⁶² The

entanglement of the electronic transitions is quantified by the effective number of the entangled states⁶³ defined as:

$$Z_{HE} = 1 / \prod_i \lambda_i^{\lambda_i}, \quad (3)$$

where λ_i are the renormalized squares of singular values of the one-particle transition density matrix

$$\lambda_i = \frac{(\sigma_i)^2}{\sum_i (\sigma_i)^2} \quad (4)$$

giving the weights of natural hole-particle configurations in each transition. Z_{HE} reflect both spin and spatial entanglement. An excited state produced by an excitation of a single unpaired electron (as in H or Li atom) has $Z_{HE}=1$ (no entanglement); a singlet excited state corresponding to an excitation between a single pair of spatial orbitals (such as HOMO-LUMO excitation in H₂) has $Z_{HE}=2$ (two entangled states due to spin coupling); and an excited state in an idealized bi-chromophoric system (two H₂ far apart) can have maximum $Z_{HE}=4$. An excited state in a stretched H₂ (or Li₂) has also $Z_{HE}=4$, reflecting the entanglement between local excitations of the two separated but entangled chromophores. Thus, diradical character would manifest itself by an increased Z_{HE} . (Special care is needed when extracting S_{HE} and Z_{HE} from spin-integrated density matrices; see the SI for details. We also note that Z_{HE} are similar to other descriptors of collectivity, such as participation ratios.)

All electronic structure calculations were performed using the *Q-Chem* package;^{64,65} the wavefunction analysis was carried out using *libwfa* library.⁵⁹ The computational details are described in the SI.

Before proceeding to discuss the electronic structure of homosymmetric ACCA molecules, we first examine a simpler case of two weakly interacting Li atoms, sufficiently far apart such that the underlying wavefunction exhibits strong diradical character. In this pedagogical example, the two unpaired electrons can only interact directly through space in the absence of a linker.

The computed EOM-DEA-CCSD energy diagram follows the expectations from Hückel’s molecular orbital theory (Figure 3A). The weak through-space interaction in Li₂ splits the atomic ²P state into four states: the pair of ¹Σ_u⁺ and ¹Σ_g⁺ states separated by 0.16 eV and

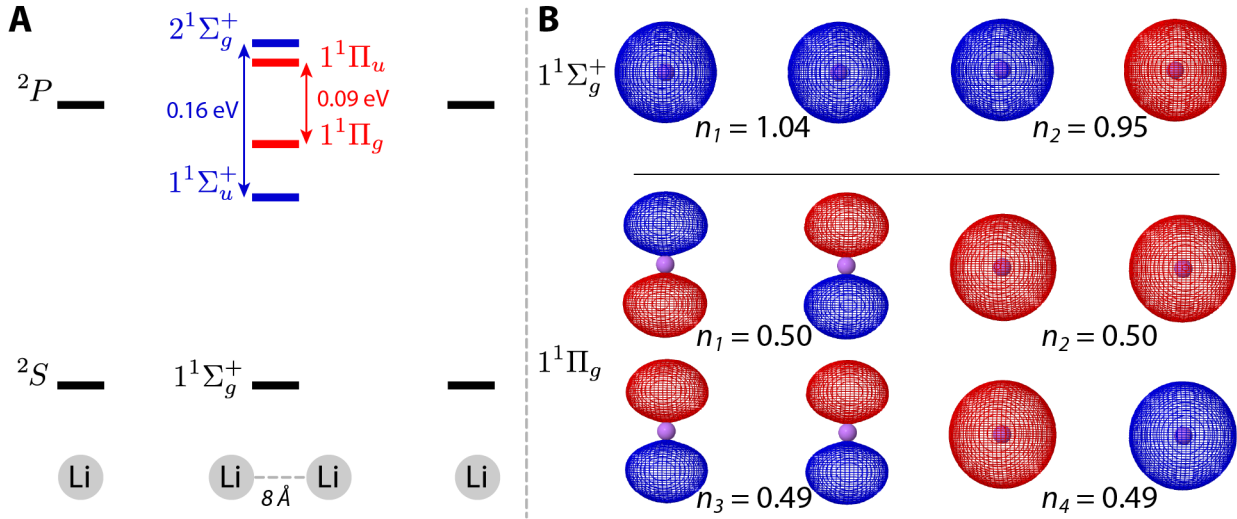


Figure 3: Energy diagram of Li₂ (A) and natural orbitals with their occupations of ¹Σ_g⁺ and ¹Π_g states (B) calculated using EOM-DEA-CCSD/aug-cc-pVTZ.

the pair of ¹Π_g and ¹Π_u states separated by 0.09 eV. The difference in splitting in the two pairs of states is consistent with the different orbital overlap between the *p*-orbitals oriented parallel or perpendicular to the Li-Li axis. Figure 3B shows frontier natural orbitals and their occupations in the ¹Σ_g⁺ and ¹Π_g states as two representative examples. In the ground ¹Σ_g⁺ state, the occupation numbers are very close to those of a nearly perfect diradical (covalent) wavefunction yielding $n_{u,nl} = 1.99$. The excited ¹Π_g state is characterized by four half-filled orbitals giving rise to $n_{u,nl} = 2.25$.

The structure of the triplet manifold parallels the singlet states, with the singlet-triplet gaps in the range of 0.00-0.02 eV (Table S2 in SI), further illustrating vanishing interaction between the two electrons. The electronic transitions in dimers or bi-chromophoric systems can be understood by using the exciton model,⁶⁶⁻⁶⁹ which describes the electronic states of the dimer as linear combinations of the monomeric states. When applied to a homsymmetric diradical, the model predicts that one of the states in *g/u* pair is dark and the other is bright, with the oscillator strength doubled relative to an isolated radical. As the ground state in Li₂ is of *gerade* symmetry, all *g* states are dark and *u* states are bright. The effective number of entangled states Z_{HE} in these four lowest-energy transitions is 4.0 due to spin- and space-

entanglement of electronic excitation, as compared to $Z_{HE} = 1.0$ in an isolated Li atom and $Z_{HE} \approx 2.0$ in Li_2 around the equilibrium geometry. In addition to the singly excited states of covalent character, there are also higher-lying doubly excited states of covalent character, as well as the manifold of the singly and doubly excited ionic states.

In a hypermetallic molecule of the ACCA type, one of the two valence electrons of each alkaline earth metals is transferred to the linker, giving rise to strongly ionic AC bonds and two unpaired electrons, each localized at the respective metal center, making ACCA analogous to the two alkali metals separated by a large distance. Below we examine the electronic structure of ACCH and ACCA with varied metal ($A = \text{Mg}, \text{Ca}, \text{Sr}$) and compare with electronic structure of Li_2 .

Considering electronic structure of ACCH, in the ground $X^2\Sigma^+$ state the unpaired electron is localized at the metal occupying the hybridized $s\sigma$ - $p\sigma$ orbital (see a representative example of the Dyson orbitals of MgCCH in Figure 4A). Upon excitation to the higher $1^2\Pi$ and $2^2\Sigma^+$ states, the electron remains localized at the metal and occupies the hybridized $p\pi$ - $d\pi$ and $p\sigma$ - $d\sigma$ orbitals, respectively. The orbital hybridization arises due to the presence of the negatively charged ligand and can be reproduced by perturbatively adding a point-charge potential to the Hamiltonian of a hydrogen-like atom.²⁹

While the electron remains largely localized at the metal, the minor leakage to the ligand is always present, leading to slightly non-diagonal FCFs that depend on both alkaline earth metal and the ligand.²⁹ For example, although the Dyson orbitals in the three ACCHs look similar (Figure S1 in the SI), in MgCCH the unpaired electron resides closer to the CCH moiety as compared to CaCCH and SrCCH . Indeed, Mulliken’s population analysis confirms that the partial charge at the metal increases from 0.21 in MgCCH to 0.39 in CaCCH to 0.54 in SrCCH , suggesting that the A-C bond becomes more ionic and the unpaired electron more localized at the metal. This conclusion is further confirmed by the fact that among the three alkaline earth metals the ionization energy is the largest for Mg atom and the smallest for Sr (Table S3 in the SI). Accordingly, excitation energies to $1^2\Pi$ and $2^2\Sigma^+$ in ACCH decrease as the alkaline metal is changed from Mg to Ca to Sr (Figure 4B)— a trend that is also observed in the properties

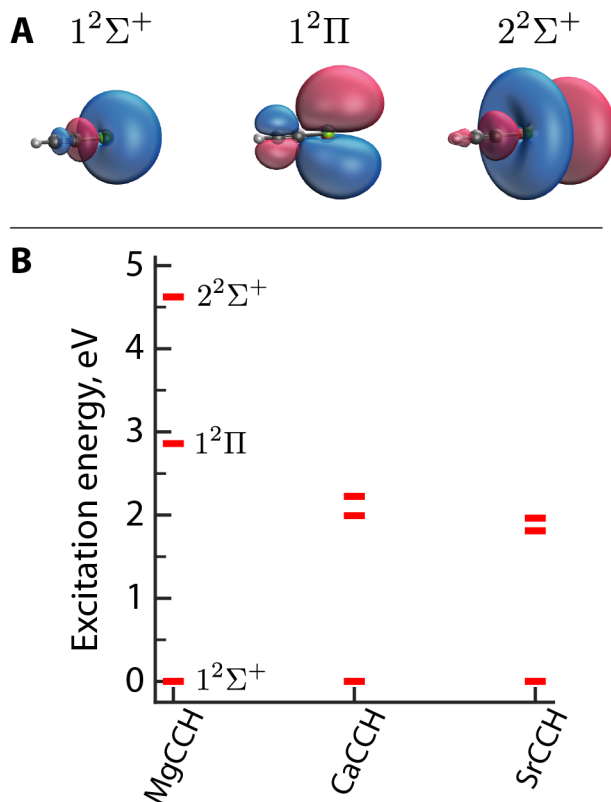


Figure 4: Dyson orbitals of three low-lying electronic states of MgCCH (A) and energy diagrams of ACCH (B) calculated using EOM-EA-CCSD/aug-cc-pwCVTZ(-PP)[Mg,Ca,Sr]/cc-pVTZ[C,H]. See Figure S1 in the SI for the Dyson orbitals of all three ACCHs. Numeric values of the excitation energies and oscillator strengths are given in Table S4 in the SI.

of the ACCA molecules.

In ACCA, the two alkaline earth metals are rigidly held at the distance of 5.3-6.1 Å (depending on the metal) by the acetylene linker. In all three systems, the singlet is the ground state. The singlet-triplet gap is small and decreases in the Mg→Ca→Sr series (0.016–0.003–~0 eV). The trends in the singlet-triplet gaps indicate strong diradical character and weak bonding interactions between the unpaired electrons. Drawing from the studies of the organic diradicals and triradicals,^{42,53} the differences in the equilibrium geometries of singlet and triplet states can also be used to quantify the extent of the diradical character. In molecules with large diradical character, the geometries of singlet and triplet states are quite similar, while in closed-shell molecules the two geometries differ significantly. The EOM-SF calculations showed that the geometries of the ground $X^1\Sigma_g^+$ and $1^3\Sigma_u^+$ states of all three ACCAs are nearly identical (Table S7 in SI), reflecting a weak interaction between the two unpaired electrons and large diradical

character.

To quantify the strength of the interaction between two unpaired electrons in a diradical in terms of thermochemical quantities, we consider the diradical stabilization energy (DSE)—an energy of a hypothetical isodesmic reaction in which two interacting radical centers are separated into two molecules.^{42,53,70} In the case of ACCB, such a reaction is



Interestingly, all computed DSEs are negative and increase in magnitude in the Mg→Ca→Sr series from -1 kcal/mol to -6 kcal/mol (Table S8). This is puzzling, because in organic diradicals only positive DSEs, indicating stabilizing interaction of the radical centers, were observed and because singlet–triplet gaps in ACCA indicate weak bonding interactions. We attribute negative DSEs to strongly ionic nature of the AC bonds, which results in negative charges of the acetylene linker, resulting in the strong Coulomb repulsion. The analysis of Mulliken’s charges shows increased ionic character in the Mg→Ca→Sr series, which correlates with increasingly negative DSEs (Table S8). If the Coulomb contribution is removed from DSE, then the covalent component is positive for all ACCA molecules and varies from 7-23 kcal/mol, which is in the range typical for organic diradicals.^{42,53}

Finally, as in the case of Li₂, we consider natural orbitals as a tool to interpret the electronic structures of ACCAs. Figure 5A shows two frontier natural orbitals and their occupations for the ground $X^1\Sigma_g^+$ state of MgCCMg; natural orbitals of CaCCCa and SrCCSr are shown in Figure S2 in the SI. In all three molecules, the antibonding natural orbital has a higher occupation number than the bonding orbital in contrast to the case of Li₂, where, in the agreement with the molecular orbital theory, the bonding natural orbital lies below the antibonding orbital. Such an effect of the flipped orbital ordering has been observed in systems where the (indirect) through-bond interaction between electrons dominates a weak (direct) through-space interaction; for example, it is clearly seen in *para*-benzyne^{44,45} diradical and dihydroanthracene cation radical.⁷¹ Indeed, orbital hybridization induced by the negatively charged linker directs

the distribution of the two electrons away from each other, thus minimizing the orbital overlap and through-space interaction.

The occupation numbers in all three ACCAs are very close to those of a perfectly diradical wavefunction (i.e., $n_1 = n_2 = 1$) and, correspondingly, the Head-Gordon’s indices are close to the limiting value of 2 (Table S4 in SI). The observed small deviations from the perfect diradical values reflect that the interaction between two unpaired electrons is weak but is not negligible. As such, the electronic wavefunction of the $X^1\Sigma_g^+$ state in all three ACCA molecules is dominated by the covalent configuration with a small contribution from the ionic (charge-resonance) configuration. In contrast, the $X^3\Sigma_u^+$ state is, as expected, of a pure covalent character with the $n_{u,nl} = 2.00$. The singlet-triplet energy gaps do not exceed 0.02 eV, further indicating the weak interaction between the two unpaired electrons.

Interestingly, the covalent character of the ground state wavefunction of ACCAs increases when the metal is changed from Mg to Ca to Sr, as evidenced by the increasing $n_{u,nl}$ (Table S4 in SI). This observation is consistent with the increasing ionic character of A-C bonds in ACCA as the partial charge on metal increases from 0.21 in MgCCMg to 0.29 in CaCCCa to 0.47 in SrCCSr. In parallel, the singlet-triplet gap decreases from 0.016 eV in MgCCMg to 0.003 eV in CaCCCa and completely vanishes in SrCCSr, further supporting that the interaction between two electrons decreases as the metal changes.

The structure of the excited states in all three ACCA follows the same pattern as in Li_2 discussed above. The $1^2\Pi$ and $2^2\Sigma^+$ states of the single-center ACCH are split into the $\Pi_{g/u}$ and $\Sigma_{u/g}^+$ pairs in both singlet and triplet manifolds in ACCA (Figure 5B). Due to the symmetry, one of the states is dark and the other is bright with the oscillator strength doubled relative to ACCH. The energy splittings are relatively small, within 0.02-0.1 eV, reflecting a weak interaction between two electrons in the excited states. In MgCCMg, a pair of the ionic (charge-resonance) states lies in between the $^1\Pi_{g/u}$ and $^1\Sigma_{u/g}^+$ pairs, whereas in CaCCCa and SrCCSr these states appear above $^1\Pi_{g/u}$ and $^1\Sigma_{u/g}^+$ pairs (compare positions of blue and black bars in Figure 5B). For all considered transitions, the number of entangled states is 3.8-4.5 (Table S4 in SI).

Similarly to the case of Li_2 , the single-electron excitation may result in four partially occupied orbitals as can be concluded from the values of $n_{u,nl}$ that are close to 2.25 (Table S4 in SI) and the natural orbitals of $1^1\Pi_g$ state in MgCCMg are shown as a representative example in Figure 5A. Interestingly, the ordering of the occupations in natural orbitals in MgCCMg is opposite to that in CaCCCa and SrCCSr (Figure S2 in SI), yet matches those in Li_2 . These observations highlight that the through-space orbital interactions in MgCCMg are more dominant than in CaCCCa and SrCCSr due to the extended delocalization of the unpaired electron as can be confirmed by visual inspection of the Dyson orbitals of MgCCH (Figure 4A) and natural orbitals in MgCCMg (Figure 5A).

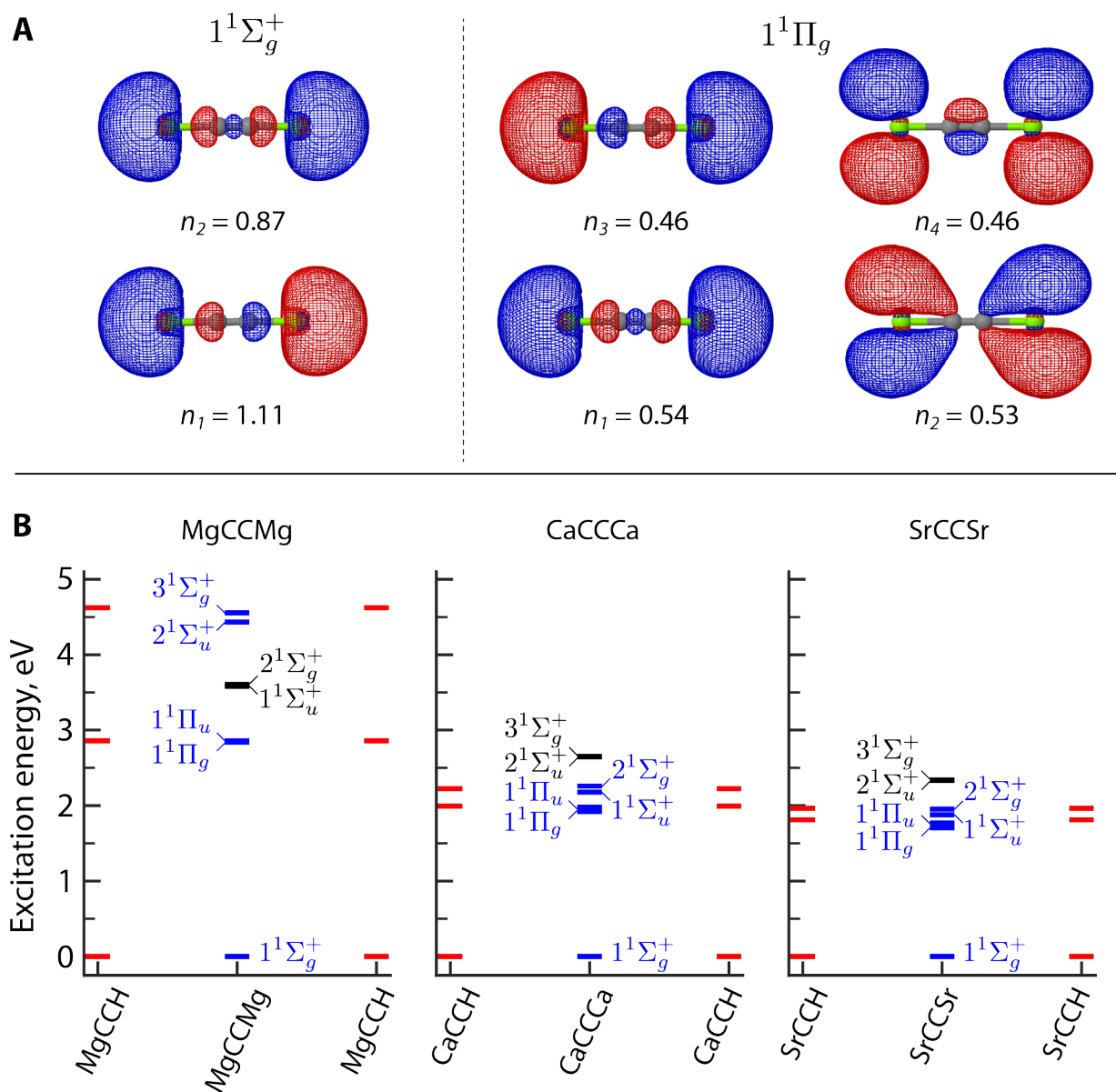


Figure 5: Natural orbitals (isovalue 0.02) of the $1^1\Sigma_g^+$ and $1^1\Pi_g$ states of MgCCMg (A) and energy diagrams of ACCA and corresponding ACCH (B) calculated using EOM-DEA-CCSD/aug-cc-pwCVTZ(-PP)[Mg,Ca,Sr]/cc-pVTZ[C,H]. In panel B, red bars correspond to three low-lying states of ACCH, blue bars correspond to the states that originate from the splitting of the corresponding states in ACCH, black bars correspond to the ionic (charge-resonance) states of ACCA. Numeric values of the excitation energies, oscillator strengths, and Head-Gordon's indices in singlet and triplet manifolds are given in Table S4 in SI.

Switching to ACCBs, Figure 6A shows two frontier natural orbitals and their occupations for the ground $X^1\Sigma^+$ state of MgCCCa; natural orbitals of MgCCSr and CaCCSr are shown in Figure S3 in SI. Similarly to ACCA, the antibonding natural orbital has a higher occupation number than the bonding orbital reflecting a considerable role of through-bond interactions.

The occupation numbers in all three ACCBs across all covalent states are either close or match exactly those of a perfectly diradical wavefunction and, correspondingly, the Head-Gordon’s indices approach their limiting values of 2 (Table S5 in SI). In particular, in the ground state $n_{u,nl}$ is in the range of 1.96-1.99 suggesting that the interaction between two electrons is weak but non-negligible. Accordingly, singlet-triplet gap varies in the range of 0.008-0.002 eV depending on the particular combination of alkaline earth metals.

In contrast to the ground state, in the $1^1\Pi$ state, $n_{u,nl} = 2.00$ in all three molecules suggesting a pure diradical character of the wavefunction. This is further supported by the natural orbitals analysis. Natural orbitals of MgCCCa displayed in Figure 6A show that in the $1^1\Pi$ state, the electron on Mg side is in its local ground Σ^+ state, whereas the second electron is in the locally excited Π state. Specifically, the occupation number of both natural orbitals is 0.99 and the visual appearance of the natural orbitals is similar to the Dyson orbitals of the corresponding states in MgCCH and CaCCH.

As the transition to the $1^1\Pi$ state in MgCCCa is localized on Ca, the excitation energy and oscillator strength are close to those associated with the transition to the $1^2\Pi$ state in CaCCH. In particular, excitation energy and oscillator strength are lowered by 0.009 eV and 0.014, respectively, in MgCCCa as compared to CaCCH, reflecting small but noticeable interaction. Generally, for heavier alkaline earth metals and higher-lying states, the change in the excitation energy in ACCB relative to the respective ACCH, tends to increase due to more diffuse character of the corresponding orbitals. For example, in CaCCSr excitation energy to $2^1\Delta$ state is shifted by 0.079 eV relative to the excitation energy to $1^2\Delta$ state in CaCCH (Table S5 in SI). Inspection of the energy diagrams in Figure 6B shows that the spectra of ACCB molecules corresponds to the sum of the ACCH and BCCH spectra with the presence of the ionic states. The effective number of entangled states for these transitions is smaller than in ACCA, reflecting

an independence in the electronic excitation of each electron in ACCB (compare Z_{HE} in Table S4 and S5 in SI).

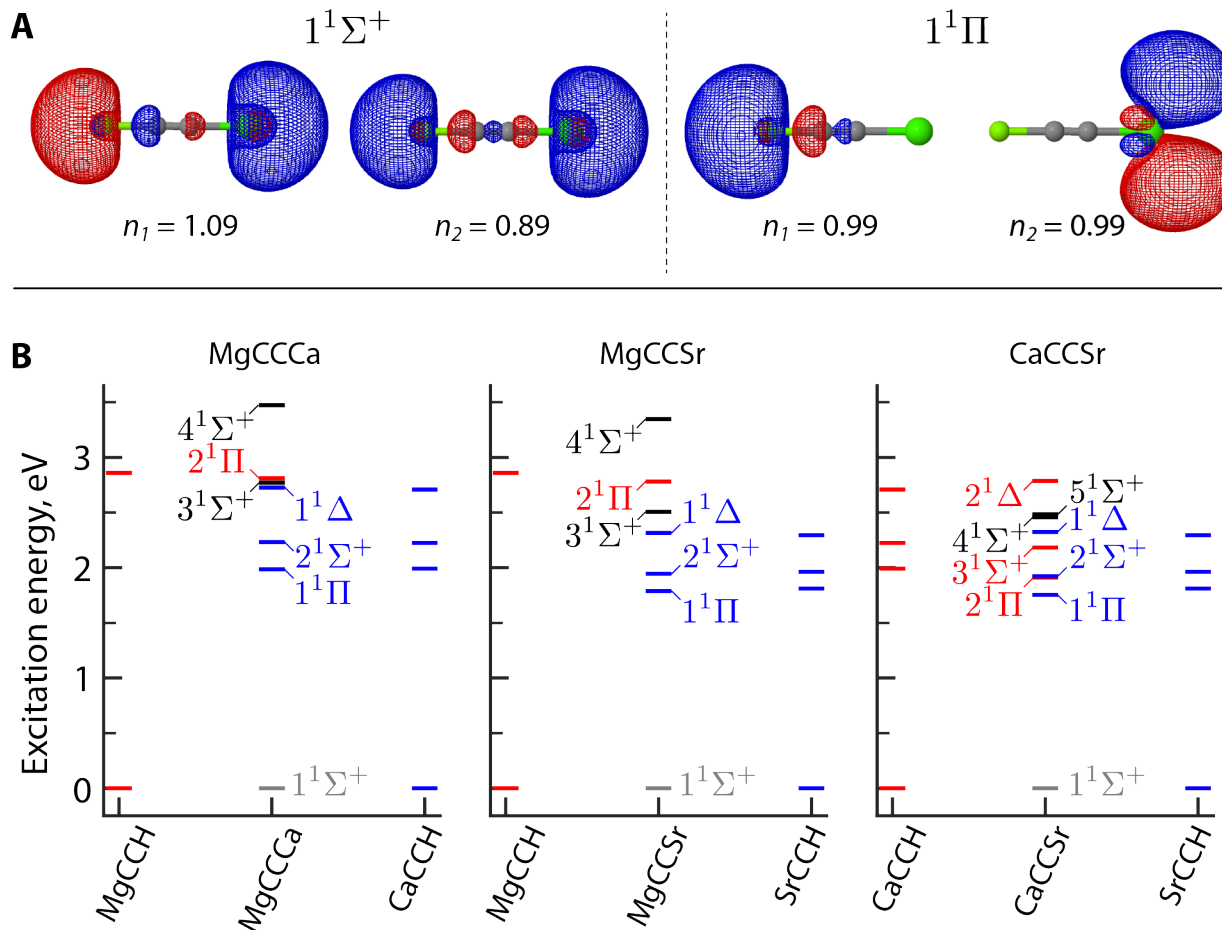


Figure 6: Natural orbitals (isovalue 0.02) of the $1^1\Sigma^+$ and $1^1\Pi$ states of MgCCCa (A) and energy diagrams of ACCB and corresponding ACCH (B) calculated using EOM-DEA-CCSD/aug-cc-pwCVTZ(-PP)[Mg,Ca,Sr]/cc-pVTZ[C,H]. In panel B, red and blue bars correspond to the low-lying states of respective ACCH, black bars correspond to the ionic states of ACCB. Numeric values of the excitation energies, oscillator strengths, and Head-Gordon's indices in singlet and triplet manifolds are given in Table S5 in SI.

In conclusion, using EOM-DEA-CCSD approach we investigated the electronic structure of hypermetallic molecules with two alkaline earth metals separated by the acetylene linker—a promising platform for applications in QIS and precision measurements. We showed that the electronic structure of homosymmetric molecules closely resembles that of two alkali metals, however, the presence of the acetylene linker introduces distinct features to their electronic structure properties that are not present in the diatomic analogues.

First, negatively charged carbon atoms in the linker polarize both unpaired electrons via orbital hybridization turning them away from each other and thus minimizing the through-space interaction between the electrons.

Second, the communication between two electrons occurs largely through the acetylene linker via through-bond interaction rather than through space as evident from the ordering of the natural orbitals. However, excitation to the higher-lying (Rydberg) states or design of diradicals with Rydberg character in the ground state may facilitate through-space interactions. Despite these difference, the spectrum of ACCA molecules is similar to that of Li_2 and, in addition to the ionic states, consists from the pairs of dark and bright states. Noteworthy, the oscillator strength of these bright states is doubled as compared to the monomeric ACCH.

Third, because of the strongly ionic character of A-C bonds, ACCB show negative DSEs, despite weak stabilizing interactions between the unpaired electrons manifested in singlets being below triplets. We attribute the origin of negative DSEs to Coulomb repulsion between carbons in the charged acetylenic linker. When the Coulomb repulsion contribution is removed, DSEs become positive, reflecting bonding interactions between the unpaired electrons, and their magnitudes fall in a range typical for molecules with strong diradical character ($\sim 0\text{-}23$ kcal/mol).

In ACCB molecules, the overall spectrum corresponds to the sum of the ACCH and BCCH spectra with the presence of the ionic states. Natural orbital analysis of the excited states showed that the two electrons act independently: upon excitation one of the electron remains in the local ground state, while the second electron becomes locally excited. Yet, the interaction between two electrons cannot be considered negligible as the excitation energies in ACCB are

shifted by 0.01-0.08 eV as compared to the corresponding ACCH. Analysis of the entanglement further highlights different nature of electronic transitions in ACCA and ACCB. The number of entangled states is generally close to 4 in ACCA molecules, and is reduced in ACCB, reflecting the independent nature of the electronic excitation of each unpaired electron in ACCB.

This work highlights the rich electronic structure of hypermetallic molecules that may give rise to novel applications in QIS, precision measurements, and ultra-cold chemistry. Future studies will involve the study of molecules with varied linkers and the exploration of the suitability of these molecules for laser cooling. A particular interest also lies in the investigations of the doubly excited states and electronic structure properties of the Rydberg states.

Acknowledgments

This study was funded through the “Molecules Functionalized with Optical Cycling Centers” collaboration, supported by the U.S. Department of Energy (Award DE-SC0019245). A.I.K. is also a grateful recipient of the Simons Fellowship in Theoretical Physics and of the Mildred Dresselhaus Award, which supported her sabbatical stay in Germany. We thank Professor Felix Plasser (Loughborough University) for illuminating discussions on the subject of entanglement.

Conflicts of interest

A.I.K. is the President and a part-owner of Q-Chem, Inc.

References

- (1) DeMille, D. Quantum computation with trapped polar molecules. *Phys. Rev. Lett.* **2002**, *88*, 067901.
- (2) Blackmore, J. A.; Caldwell, L.; Gregory, P. D.; Bridge, E. M.; Sawant, R.; Aldegunde, J.; Mur-Petit, J.; Jaksch, D.; Hutson, J. M.; Sauer, B. E.; et al, Ultracold molecules for quantum simulation: rotational coherences in CaF and RbCs. *Quantum Sci. Technol.* **2018**, *4*, 014010.
- (3) Hudson, E. R.; Campbell, W. C. Dipolar quantum logic for freely rotating trapped molecular ions. *Phys. Rev. A* **2018**, *98*, 040302.
- (4) Yu, P.; Cheuk, L. W.; Kozyryev, I.; Doyle, J. M. A scalable quantum computing platform using symmetric-top molecules. *New J. Phys.* **2019**, *21*, 093049.
- (5) Augenbraun, B. L.; Lasner, Z. D.; Frenett, A.; Sawaoka, H.; Miller, C.; Steimle, T. C.; Doyle, J. M. Laser-cooled polyatomic molecules for improved electron electric dipole moment searches. *New J. Phys.* **2020**, in press; DOI: <https://doi.org/10.1088/1367-2630/ab687b>.
- (6) Kozyryev, I.; Hutzler, N. R. Precision measurement of time-reversal symmetry violation with laser-cooled polyatomic molecules. *Phys. Rev. Lett.* **2017**, *119*, 133002.
- (7) Yang, T.; Li, A.; Chen, G. K.; Xie, C.; Suits, A. G.; Campbell, W. C.; Guo, H.; Hudson, E. R. Optical control of reactions between water and laser-cooled Be⁺ ions. *J. Phys. Chem. Lett.* **2018**, *9*, 3555–3560.
- (8) Hutson, J. M. Ultracold chemistry. *Science* **2010**, *327*, 788–789.
- (9) Bell, M. T.; Softley, T. P. Ultracold molecules and ultracold chemistry. *Mol. Phys.* **2009**, *107*, 99–132.

- (10) Van der Straten, P.; Metcalf, H. *Atoms and molecules interacting with light: Atomic physics for the laser era*; Cambridge University Press, 2016.
- (11) Quemener, G.; Julienne, P. S. Ultracold molecules under control! *Chem. Rev.* **2012**, *112*, 4949–5011.
- (12) Rosa, M. D. D. Laser-cooling molecules. *Eur. Phys. J. D* **2004**, *31*, 395–402.
- (13) Shuman, E. S.; Barry, J. F.; DeMille, D. Laser cooling of a diatomic molecule. *Nature* **2010**, *467*, 820.
- (14) Barry, J. F.; McCarron, D. J.; Norrgard, E. B.; Steinecker, M. H.; DeMille, D. Magneto-optical trapping of a diatomic molecule. *Nature* **2014**, *512*, 286.
- (15) Hummon, M. T.; Yeo, M.; Stuhl, B. K.; Collopy, A. L.; Xia, Y.; Ye, J. 2D magneto-optical trapping of diatomic molecules. *Phys. Rev. Lett.* **2013**, *110*, 143001.
- (16) Collopy, A. L.; Ding, S.; Wu, Y.; Finneran, I. A.; Anderegg, L.; Augenbraun, B. L.; Doyle, J. M.; Ye, J. 3D magneto-optical trap of yttrium monoxide. *Phys. Rev. Lett.* **2018**, *121*, 213201.
- (17) Zhelyazkova, V.; Cournol, A.; Wall, T. E.; Matsushima, A.; Hudson, J. J.; Hinds, E. A.; Tarbutt, M. R.; Sauer, B. E. Laser cooling and slowing of CaF molecules. *Phys. Rev. A* **2014**, *89*, 053416.
- (18) Anderegg, L.; Augenbraun, B. L.; Bao, Y.; Burchesky, S.; Cheuk, L. W.; Ketterle, W.; Doyle, J. M. Laser cooling of optically trapped molecules. *Nat. Phys.* **2018**, *14*, 890–893.
- (19) Truppe, S.; Williams, H. J.; Hambach, M.; Caldwell, L.; Fitch, N. J.; Hinds, E. A.; Sauer, B. E.; Tarbutt, M. R. Molecules cooled below the Doppler limit. *Nat. Phys.* **2017**, *13*, 1173.
- (20) Lim, J.; Almond, J. R.; Trigatzis, M. A.; Devlin, J. A.; Fitch, N. J.; Sauer, B. E.; Tarbutt, M. R.; Hinds, E. A. Laser cooled YbF molecules for measuring the electron’s electric dipole moment. *Phys. Rev. Lett.* **2018**, *120*, 123201.

- (21) Wells, N.; Lane, I. C. Electronic states and spin-forbidden cooling transitions of AlH and AlF. *Phys. Chem. Chem. Phys.* **2011**, *13*, 19018–19025.
- (22) Nguyen, J. H. V.; Viteri, C. R.; Hohenstein, E. G.; Sherrill, C. D.; Brown, K. R.; Odom, B. Challenges of laser-cooling molecular ions. *New J. Phys.* **2011**, *13*, 063023.
- (23) Gao, Y.; Gao, T. Laser cooling of the alkaline-earth-metal monohydrides: Insights from an *ab initio* theory study. *Phys. Rev. A* **2014**, *90*, 052506.
- (24) Wan, M.-J.; Shao, J.-X.; Huang, D.-H.; Jin, C.-G.; Yu, Y.; Wang, F.-H. Laser cooling of BeCl and BeBr molecules in an *ab initio* method. *Phys. Chem. Chem. Phys.* **2015**, *17*, 26731–26739.
- (25) Li, C.; Li, Y.; Ji, Z.; Qiu, X.; Lai, Y.; Wei, J.; Zhao, Y.; Deng, L.; Chen, Y.; Liu, J. Candidates for direct laser cooling of diatomic molecules with the simplest $^1\Sigma$ - $^1\Sigma$ electronic system. *Phys. Rev. A* **2018**, *97*, 062501.
- (26) Isaev, T. A.; Zaitsevskii, A. V.; Eliav, E. Laser-coolable polyatomic molecules with heavy nuclei. *J. Phys. B* **2017**, *50*, 225101.
- (27) Gaul, K.; Berger, R. *Ab initio* study of parity and time-reversal violation in laser-coolable triatomic molecules. *Phys. Rev. A* **2020**, *101*, 012508.
- (28) Li, M.; Kłos, J.; Petrov, A.; Kotochigova, S. Emulating optical cycling centers in polyatomic molecules. *Commun. Phys.* **2019**, *2*.
- (29) Ivanov, M. V.; Bangerter, F. H.; Krylov, A. I. Towards a rational design of laser-coolable molecules: Insights from equation-of-motion coupled-cluster calculations. *Phys. Chem. Chem. Phys.* **2019**, *21*, 19447–19457.
- (30) Kozyryev, I.; Baum, L.; Matsuda, K.; Augenbraun, B. L.; Anderegg, L.; Sedlack, A. P.; Doyle, J. M. Sisyphus laser cooling of a polyatomic molecule. *Phys. Rev. Lett.* **2017**, *118*, 173201.

- (31) Isaev, T. A.; Berger, R. Polyatomic candidates for cooling of molecules with lasers from simple theoretical concepts. *Phys. Rev. Lett.* **2016**, *116*, 063006.
- (32) Kozyryev, I.; Baum, L.; Matsuda, K.; Doyle, J. M. Proposal for laser cooling of complex polyatomic molecules. *ChemPhysChem* **2016**, *17*, 3641–3648.
- (33) O’Rourke, M. J.; Hutzler, N. R. Hypermetallic Polar Molecules for Precision Measurements. *Phys. Rev. A* **2019**, *100*, 022502.
- (34) Merritt, J. M.; Bondybey, V. E.; Heaven, M. C. Spectroscopy, structure, and ionization energy of BeOBe. *J. Phys. Chem. A* **2009**, *113*, 13300–13309.
- (35) Antonov, I. O.; Barker, B. J.; Heaven, M. C. Pulsed-field ionization zero electron kinetic energy spectrum of the ground electronic state of BeOBe⁺. *J. Chem. Phys.* **2011**, *134*, 044306.
- (36) Ostojić, B.; Bunker, P. R.; Schwerdtfeger, P.; Assadollahzadeh, B.; Jensen, P. The predicted spectrum of the hypermetallic molecule MgOMg. *Phys. Chem. Chem. Phys.* **2011**, *13*, 7546–7553.
- (37) Ostojić, B.; Bunker, P. R.; Schwerdtfeger, P.; Gertych, A.; Jensen, P. The predicted infrared spectrum of the hypermetallic molecule CaOCa in its lowest two electronic states $X^1\Sigma_g^+$ and $a^3\Sigma_u^+$. *J. Molec. Struct.* **2012**, *1023*, 101–107.
- (38) Ostojić, B.; Jensen, P.; Schwerdtfeger, P.; Bunker, P. R. The predicted spectrum and singlet–triplet interaction of the hypermetallic molecule SrOSr. *J. Phys. Chem. A* **2013**, *117*, 9370–9379.
- (39) Puri, P.; Mills, M.; Schneider, S.; Simbotin, I.; Montgomery, J. A.; Côté, R.; Suits, A. G.; Hudson, E. R. Synthesis of mixed hypermetallic oxide BaOCa⁺ from laser-cooled reagents in an atom-ion hybrid trap. *Science* **2017**, *357*, 1370–1375.
- (40) Salem, L.; Rowland, C. The electronic properties of diradicals. *Angew. Chem., Int. Ed.* **1972**, *11*, 92–111.

- (41) Bonačić-Koutecký, V.; Koutecký, J.; Michl, J. Neutral and charged biradicals, zwitterions, funnels in S_1 , and proton translocation: Their role in photochemistry, photophysics, and vision. *Angew. Chem., Int. Ed.* **1987**, *26*, 170–189.
- (42) Krylov, A. I. Triradicals. *J. Phys. Chem. A* **2005**, *109*, 10638–10645.
- (43) Krylov, A. I. In *Reviews in Comp. Chem.*; Parrill, A. L., Lipkowitz, K. B., Eds.; J. Wiley & Sons, 2017; Vol. 30; pp 151–224.
- (44) Baldrige, K. K.; Buttersby, T. R.; Clark, R. V.; Siegel, J. S. Does $\pi - \sigma - \pi$ through bond coupling significantly increase C-C bond lengths? *J. Am. Chem. Soc.* **1997**, *119*, 7048–7054.
- (45) Orms, N.; Rehn, D. R.; Dreuw, A.; Krylov, A. I. Characterizing bonding patterns in diradicals and triradicals by density-based wave function analysis: A uniform approach. *J. Chem. Theory Comput.* **2017**, *14*, 638–648.
- (46) Krylov, A. I. Equation-of-motion coupled-cluster methods for open-shell and electronically excited species: The hitchhiker’s guide to Fock space. *Annu. Rev. Phys. Chem.* **2008**, *59*, 433–462.
- (47) Bartlett, R. J. Coupled-cluster theory and its equation-of-motion extensions. *WIREs: Comput. Mol. Sci.* **2012**, *2*, 126–138.
- (48) Krylov, A. I. Size-consistent wave functions for bond-breaking: The equation-of-motion spin-flip model. *Chem. Phys. Lett.* **2001**, *338*, 375–384.
- (49) Slipchenko, L. V.; Krylov, A. I. Singlet-triplet gaps in diradicals by the spin-flip approach: A benchmark study. *J. Chem. Phys.* **2002**, *117*, 4694–4708.
- (50) Krylov, A. I. The spin-flip equation-of-motion coupled-cluster electronic structure method for a description of excited states, bond-breaking, diradicals, and triradicals. *Acc. Chem. Res.* **2006**, *39*, 83–91.

- (51) Perera, A.; Molt, R. W.; Lotrich, V. F.; Bartlett, R. J. In *Isaiah Shavitt*; Cramer, C. J., Truhlar, D. G., Eds.; A memorial festschrift from theoretical chemistry accounts; Springer, 2016; Vol. 9; pp 153–165.
- (52) Levchenko, S. V.; Wang, T.; Krylov, A. I. Analytic gradients for the spin-conserving and spin-flipping equation-of-motion coupled-cluster models with single and double substitutions. *J. Chem. Phys.* **2005**, *122*, 224106–224116.
- (53) Cristian, A. M. C.; Shao, Y.; Krylov, A. I. Bonding patterns in benzene triradicals from structural, spectroscopic, and thermochemical perspectives. *J. Phys. Chem. A* **2004**, *108*, 6581–6588.
- (54) Löwdin, P.-O. Quantum theory of many-particle systems. I. Physical interpretations by means of density matrices, natural spin-orbitals, and convergence problems in the method of configurational interaction. *Phys. Rev.* **1955**, *97*, 1474–1489.
- (55) Head-Gordon, M. Characterizing unpaired electrons from the one-particle density matrix. *Chem. Phys. Lett.* **2003**, *372*, 508–511.
- (56) Plasser, F.; Pašalić, H.; Gerzabek, M. H.; Libisch, F.; Reiter, R.; Burgdörfer, J.; Müller, T.; Shepard, R.; Lischka, H. The multiradical character of one- and two-dimensional graphene nanoribbons. *Angew. Chem., Int. Ed.* **2013**, *52*, 2581–2584.
- (57) Oana, C. M.; Krylov, A. I. Dyson orbitals for ionization from the ground and electronically excited states within equation-of-motion coupled-cluster formalism: Theory, implementation, and examples. *J. Chem. Phys.* **2007**, *127*, 234106–14.
- (58) Head-Gordon, M.; Grana, A. M.; Maurice, D.; White, C. A. Analysis of electronic transitions as the difference of electron attachment and detachment densities. *J. Phys. Chem.* **1995**, *99*, 14261 – 14270.
- (59) Plasser, F.; Wormit, M.; Dreuw, A. New tools for the systematic analysis and visualization of electronic excitations. I. Formalism. *J. Chem. Phys.* **2014**, *141*, 024106–13.

- (60) B  ppler, S. A.; Plasser, F.; Wormit, M.; Dreuw, A. Exciton analysis of many-body wave functions: Bridging the gap between the quasiparticle and molecular orbital pictures. *Phys. Rev. A* **2014**, *90*, 052521.
- (61) Mewes, S.; Plasser, F.; Krylov, A. I.; Dreuw, A. Benchmarking excited-state calculations using exciton properties. *J. Chem. Theory Comput.* **2018**, *14*, 710–725.
- (62) Plasser, F. Visualisation of electronic excited-state correlation in real space. *ChemPhotoChem* **2019**, *3*, 702–706.
- (63) Plasser, F. Entanglement entropy of electronic excitations. *J. Chem. Phys.* **2016**, *144*, 194107.
- (64) Shao, Y.; Gan, Z.; Epifanovsky, E.; Gilbert, A.T.B.; Wormit, M.; Kussmann, J.; Lange, A.W.; Behn, A.; Deng, J.; Feng, X., et al., Advances in molecular quantum chemistry contained in the Q-Chem 4 program package. *Mol. Phys.* **2015**, *113*, 184–215.
- (65) Krylov, A. I.; Gill, P. M. W. Q-Chem: An engine for innovation. *WIREs: Comput. Mol. Sci.* **2013**, *3*, 317–326.
- (66) East, A. L. L.; Lim, E. C. Naphthalene dimer: Electronic states, excimers, and triplet decay. *J. Chem. Phys.* **2000**, *113*, 8981–8994.
- (67) Levchenko, S. V.; Reisler, H.; Krylov, A. I.; Gessner, O.; Stolow, A.; Shi, H.; East, A. L. L. Photodissociation dynamics of the NO dimer. I. Theoretical overview of the ultraviolet singlet excited states. *J. Chem. Phys.* **2006**, *125*, 084301–084313.
- (68) Uhler, B.; Ivanov, M. V.; Kokkin, D.; Reilly, N.; Rathore, R.; Reid, S. A. Effect of facial encumbrance on excimer formation and charge resonance stabilization in model bichromophoric assemblies. *J. Phys. Chem. C* **2017**, *121*, 15580–15588.
- (69) Spano, F. C.; Silva, C. H- and J-aggregate behavior in polymeric semiconductors. *Annu. Rev. Phys. Chem.* **2014**, *65*, 477–500.

- (70) Lardin, H. A.; Nash, J. J.; Wenthold, P. G. Is the 1,3,5-Tridehydrobenzene Triradical a Cyclopropenyl Radical Analogue? *J. Am. Chem. Soc.* **2002**, *124*, 12612–12618.
- (71) Ivanov, M. V.; Wadumethrige, S. H.; Wang, D.; Rathore, R. Through-space or through-bond? The important role of cofaciality in orbital reordering and its implications for hole (de) stabilization in polychromophoric assemblies. *J. Phys. Chem. C* **2017**, *121*, 15639–15643.